Eur. Phys. J. B (2025)98:154
https://doi.org/10.1140/epjb/s10051-025-00993-4

THE EUROPEAN PHYSICAL JOURNAL B

Regular Article - Solid State and Materials

Exploration of pressure-induced superconductivity in CuSe-based compounds under high pressure

Ryo Matsumoto[1,a], Sayaka Yamamoto[1,2], Shintaro Adachi[3], Hiromi Tanaka[4], Toru Shinmei[5], Tetsuo Irifune[5], and Yoshihiko Takano[1,2]

[1] Research Center for Materials Nanoarchitectonics (MANA), National Institute for Materials Science, Tsukuba, Ibaraki 305-0047, Japan
[2] Graduate School of Pure and Applied Sciences, University of Tsukuba, 1-1-1 Tennodai, Tsukuba, Ibaraki 305-8577, Japan
[3] Department of Mechanical and Electrical Systems Engineering, Faculty of Engineering, Kyoto University of Advanced Science (KUAS), Kyoto 615-8577, Japan
[4] National Institute of Technology, Yonago College, Yonago, Tottori 683-8502, Japan
[5] Geodynamics Research Center, Premier Institute for Advanced Studies, Ehime University, Matsuyama, Ehime 790-8577, Japan

Received 2 April 2025 / Accepted 25 June 2025

Abstract. The replacement of conducting layers in known layered superconducting compounds is a significant challenge in the search for novel superconductors. In particular, the exploration of superconductors can be accelerated by combining the application of high pressure for modifying the crystal structure. In this study, we investigate the electrical transport properties of the layered CuSe-based compound BiOCuSe, which has the same structure as the 1111-type iron-based superconductor La(O,F)FeAs, under high pressure exceeding 80 GPa. In addition, as related CuSe-based compounds, the electrical properties of $YBi_2O_4Cu_2Se_2$ and Cu_2Se are measured under high pressure. Although no clear signatures of bulk superconductivity are observed in these CuSe-based compounds, filamentary superconductivity emerges in BiOCuSe and Cu_2Se. Given the rapid advancements in high-pressure techniques in recent years, further exploration of high-pressure effects on layered materials with novel conducting layers is expected to lead to the discovery of next-generation superconducting materials.

1 Introduction

Research on superconductors faces a critical stage in the quest for exploration of next-generation high-transition-temperature (T_c) materials. Recent advancements in high-pressure techniques have led to the discovery of new high-T_c superconductors, including hydrides [1, 2], borides [3], and nickelates [4, 5]. Notably, superconductors are often synthesized systematically following the discovery of a parent compound. For instance, after the report of superconductivity above 200 K in H_3S [1, 2], related high-T_c hydrides such as LaH_{10} [6, 7], YH_9 [8], and CeH_9 [9] were continuously discovered. To accelerate the exploration of superconducting materials, it is crucial to investigate the physical properties of unexplored compounds under high pressure, particularly by modifying conduction layers in layered superconductors to identify new parent materials.

Recently, layered CuSe-based compounds have attracted significant attention due to their superior functionalities, such as thermoelectric properties. In particular, BiOCuSe has been highlighted as a promising candidate for intermediate-temperature thermoelectric applications [10]. Although BiOCuSe is originally a semiconductor with a bandgap of 0.8 eV, its electronic properties can be tuned via Te substitution at the Se site [11], oxygen deficiency [12], and high-pressure application [13]. Interestingly, BiOCuSe adopts a layered ZrCuSiAs-type structure, which is the same as that of the 1111-type iron-based superconductor La(O,F)FeAs [14]. The electronic band structures at around Fermi energy (E_F) of BiOCuSe have been investigated by a density functional theory (DFT) [15]. The DFT calculation indicates that Cu and Se orbitals mainly contribute the valence band maximum, which

Supplementary Information The online version contains supplementary material available at https://doi.org/10.1140/epjb/s10051-025-00993-4.

[a] e-mail: MATSUMOTO.Ryo@nims.go.jp (corresponding author)

Published online: 19 July 2025

suggests the CuSe-plane in BiOCuSe is an electrical conducting layer. The investigation of the combined effects of the elemental substitution, the introduction of deficiency, and the high-pressure application is crucial for evaluating the potential emergence of superconductivity in carrier-tuned BiOCuSe and related compounds. $YBi_2O_4Cu_2Se_2$, which consists of alternating YBi_2O_4 blocking layers and Cu_2Se_2 conducting layers along one axis, has been reported as a metallic derivative of BiOCuSe [16, 17]. According to the DFT calculations, Cu and Se orbitals consist of the band crossing E_F in $YBi_2O_4Cu_2Se_2$ [17]. A high-pressure study of $YBi_2O_4Cu_2Se_2$ is particularly intriguing from the perspective of the exploration of superconducting material. The investigation of possible superconductivity in these compounds opens new vein of new group of materials such as recently discovered layered oxychalcogenide superconductor Na_2CoSe_2O [18]. Among binary Cu–Se systems, Cu_2Se is focused as a thermoelectric material because of the ultrahigh thermoelectric figure of merit (ZT), which exceeds 4.0 near the structural phase transition between α- and β-Cu_2Se in the temperature range of 340 K $< T <$ 400 K [19]. In addition, Cu_2Se exhibits diverse functionalities, including a possible charge density wave (CDW) state at low temperatures [20, 21], various crystal structures [19], and a pressure-induced electronic topological transition [22]. By analysis from DFT calculations, both Cu and Se orbital contribute to the valence band maximum [23]. The investigation of the electrical transport properties of Cu_2Se under high pressure is essential to understand deeper insight into its physical behavior. One of the key differences between these CuSe-based compounds and their isostructural Fe-based superconducting counterparts is the limited tunability of carrier concentration. In this context, the application of high pressure emerges as a promising approach to modify the electronic structure, serving as an alternative to carrier doping via elemental substitution.

In this study, we examine the emergence of pressure-induced superconductivity in the layered CuSe-based compounds BiOCuSe and its metallic derivative $YBi_2O_4Cu_2Se_2$, and binary Cu_2Se. The crystal structure and valence state of the obtained samples were characterized using X-ray diffraction (XRD) and X-ray photoelectron spectroscopy (XPS). High-pressure electrical transport measurements were performed using a diamond anvil cell (DAC) with the micro-electrodes. Structural information under high pressure was obtained from Raman spectroscopy in the DAC. Although the three CuSe-based compounds show no bulk superconductivity under examined pressure regions, we observed several anomalies due to filamentary superconductivity. Because the observation of filamentary signal indicates possible existence of superconducting phase in these materials, the insight in this study accelerates the future exploration of the superconducting family consisting of CuSe-based conducting layer.

2 Experimental procedures

A polycrystalline sample of $YBi_2O_4Cu_2Se_2$ was synthesized via a solid-state reaction in a vacuum-sealed quartz tube. The starting materials of Bi_2O_3 (98%), Y_2O_3 (99.99%), Bi_2Se_3 (99.9%), CuO (99.9%), and Cu (99.9%) were mixed in a molar ratio of Y:Bi:O:Cu:Se = 1:2:4:2:2, ground thoroughly, and pelletized under 200 MPa. The pellet of 5 mm diameter was sealed in an evacuated quartz tube, heated at 830 °C for 12 h, and then cooled in the furnace. As a byproduct, a small tip of single-crystalline BiOCuSe was obtained inside the quartz tube during the synthesis of $YBi_2O_4Cu_2Se_2$. Single crystals of Cu_2Se were grown using a similar procedure. Cu (99.9%) and Se (99.9%) were mixed in an atomic ratio of Cu:Se = 2:1 and sealed in an evacuated quartz tube. The sample was heated to 700 °C and held for 2 h, followed by an increase to 830 °C for 24 h. It was then naturally cooled to room temperature in the furnace.

The obtained products were characterized by chemical composition analysis using a scanning electron microscope (SEM) using a JSM-6010LA (JEOL). Structural analysis was performed using XRD with a MiniFlex 600 diffractometer (Rigaku) and Cu Kα radiation (wavelength = 1.5418 Å). The lattice constants of the samples were determined from the measured XRD patterns using PDIndexer [24]. The VESTA software was used for crystal structure visualization [25]. XPS analysis was conducted using the AXIS-ULTRA DLD (Shimadzu/Kratos) with monochromatic Al Kα radiation (photon energy = 1486.6 eV) under a pressure of the order in 10^{-9} Torr. The active Shirley method from COMPRO software [26] was used for a background subtraction for the XPS spectrum. The binding energy of the sample was calibrated by measuring the valence band spectrum of an Au reference in the same chamber.

Resistance–temperature (R–T) measurements were performed on the three compounds under both ambient and high pressures. At ambient pressure, a conventional four-probe method was used with Au wires and silver paste. For high-pressure measurements, an originally designed DAC with boron-doped diamond (BDD) electrodes [27, 28] and an undoped diamond (UDD) insulating layer [29] was used. The typical setup of DAC consisted of a nano-polycrystalline (NPD) [30] box-type anvil and a culet-type single crystalline anvil with a 300 μm culet. A sample was placed on the BDD electrodes of the anvil, and resistance was measured using the four-probe method. The probe current for resistance evaluation was determined from the current–voltage characteristics before measurement. The sample chamber was fabricated using a stainless-steel (316 L) gasket with a drilled hole of 200 μm in diameter. The UDD insulating layer electrically separated

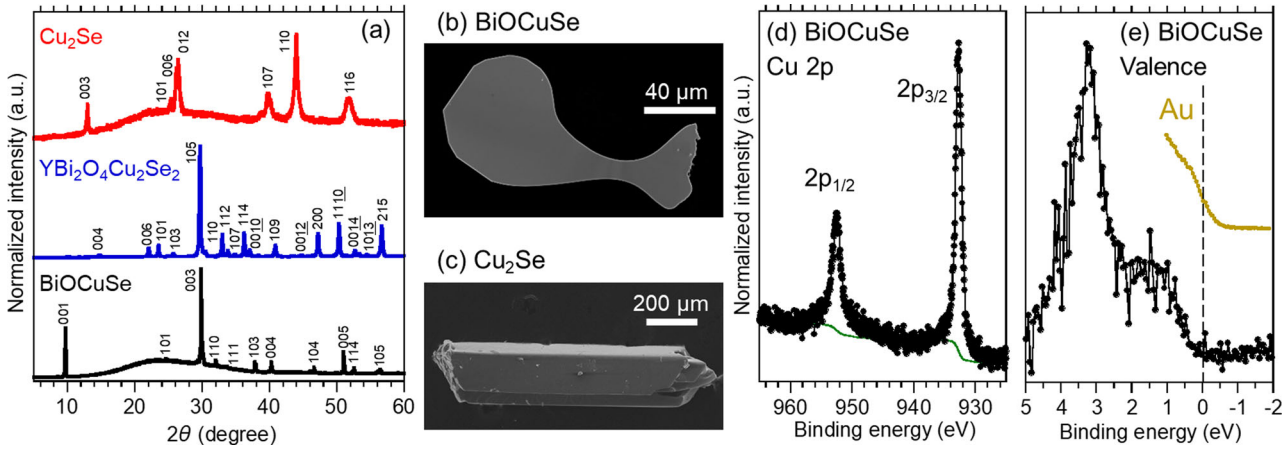

Fig. 1 **a** Powder XRD patterns of the obtained BiOCuSe, $YBi_2O_4Cu_2Se_2$ and Cu_2Se. **b** SEM images of single crystalline BiOCuSe and **c** Cu_2Se. **d** Cu 2p and **e** valence band XPS spectra in BiOCuSe

the gasket from the electrodes. Cubic boron nitride was used as the pressure-transmitting medium (PTM), with ruby powders as a pressure manometer. Such the solid PTM generally provides non-hydrostatic pressure for the sample in the case of DAC. The pressure in the sample space of the DAC was estimated by detecting the shift of peak position of ruby fluorescence [31] and the Raman spectrum of the diamond anvil [32] using an inVia Raman Microscope (RENISHAW), which is calibrated by the peak positions of these spectra at ambient pressure. The control of temperature, the measurements of sample resistance between 300 and 2 K, and the application of a magnetic field were performed using a physical property measurement system (Quantum Design).

3 Results and discussion

3.1 Characterization at ambient pressure

Figure 1a presents the XRD patterns of the obtained BiOCuSe, $YBi_2O_4Cu_2Se_2$, and Cu_2Se. Almost the all observed peaks are indexed to the known phase in these compounds such as tetragonal structure ($P4/nmm$) with the lattice constants of $a = 3.948$ and $c = 8.974$ Å in BiOCuSe, tetragonal structure ($I4/mmm$) with $a = 3.880$ and $c = 24.099$ Å in $YBi_2O_4Cu_2Se_2$, and trigonal structure (R-3 m) with $a = 4.120$ and $c = 20.533$ Å in Cu_2Se. In the case of BiOCuSe and Cu_2Se, the single crystalline samples are obtained, as shown in the SEM image of Fig. 1b, c. In the electrical transport measurements, the single crystalline samples are used for BiOCuSe and Cu_2Se. Among the elements in the synthesized samples, the valence states of Cu in $YBi_2O_4Cu_2Se_2$ and Cu_2Se are reported to have fluctuated in Cu^+ and Cu^{2+} via an XPS analysis [17, 33]. In this study, the valence states of Cu in BiOCuSe were also investigated, as shown in Fig. 1d which shows a Cu 2p core-level XPS spectrum. There are two main peaks at 952.5 and 932.7 eV corresponding to Cu $2p_{3/2}$ and $2p_{1/2}$ with the valence state of Cu^+, which is consistent with the formal charge valence of BiOCuSe. Figure 1e displays the valence band spectrum of BiOCuSe. The electronic band structure appears to approach the Fermi level, suggesting a metallic characteristic. According to previous reports, the electrical transport properties of BiOCuSe change drastically from semiconducting to metallic depending on the synthesis conditions [34]. In particular, when the synthesis temperature exceeds 730 °C, metallic BiOCuSe is obtained, which is consistent with our synthesis conditions and the observed metallic behavior.

3.2 Electrical transport properties at ambient pressure

Figure 2 presents the R–T curves of (a) BiOCuSe, (b) $YBi_2O_4Cu_2Se_2$, and (c) Cu_2Se at ambient pressure. BiOCuSe exhibits a positive slope in R–T curve from 300 to 50 K, followed by a slight upturn below 50 K. This metallic behavior is consistent with the XPS analysis, which indicates that the valence band crosses the Fermi level. The upturn is considered to be influence from slight amount of Cu deficiency in metallic BiOCuSe [10]. Similarly, $YBi_2O_4Cu_2Se_2$, known as a metallic derivative of BiOCuSe, displays metallic conduction without any noticeable anomalies. Cu_2Se also exhibits metallic behavior; however, a hump-like anomaly appears around 120 K, which is attributed to the formation of a CDW ground state [20, 21]. In all the examined CuSe-based materials of BiOCuSe, $YBi_2O_4Cu_2Se_2$, and Cu_2Se, no superconductivity is observed at ambient pressure.

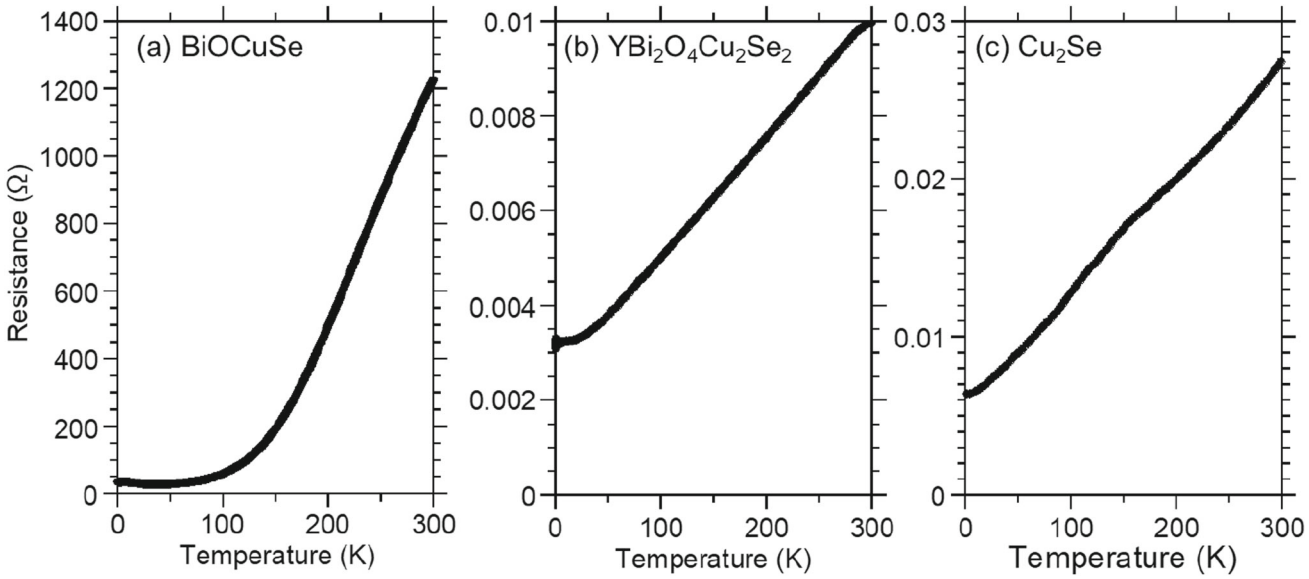

Fig. 2 Temperature dependence of electrical resistance of **a** BiOCuSe, **b** $YBi_2O_4Cu_2Se_2$, and **c** Cu_2Se at ambient pressure

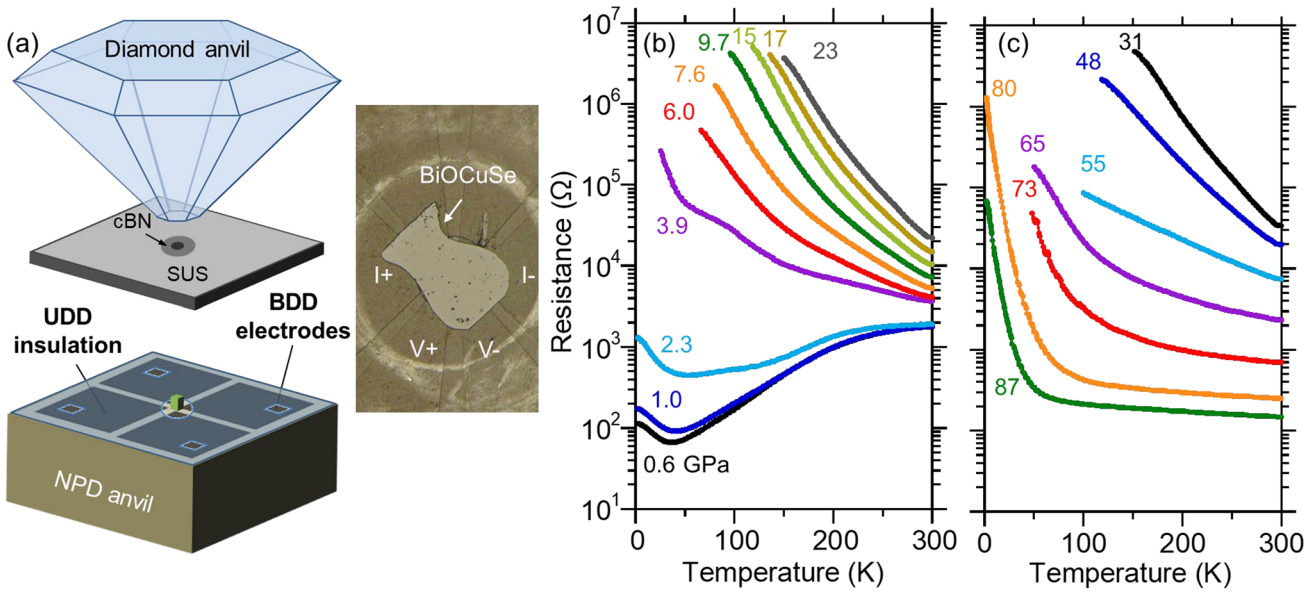

Fig. 3 **a** Typical configuration of diamond anvil cell with boron-doped diamond (BDD) electrodes and undoped diamond (UDD) insulating layer. The attached photo is a microscope image of the typical sample, such as BiOCuSe. **b** Temperature dependence of electrical resistance in BiOCuSe under various pressures up to 23 GPa and **c** 87 GPa

4 High-pressure effects

4.1 BiOCuSe

Figure 3a illustrates a typical configuration of the DAC with the BDD electrodes and the UDD insulating layer. As shown in the attached microscope image, a small piece of the sample is placed on the BDD electrodes. Upon compression, the sample and electrodes establish electrical contact, allowing for R–T measurements under high pressure, as presented in Fig. 3b, c. At the lowest pressure of 0.6 GPa, BiOCuSe exhibits metallic behavior with a slight upturn below 50 K, consistent with its transport properties at ambient pressure. However, as pressure increases to 3.9 GPa, the absolute resistance rises significantly, and the R–T curve changes to semiconducting behavior. With further compression up to 23 GPa, the semiconducting nature becomes more pronounced. Interestingly, above 31 GPa, the resistance begins to decrease unexpectedly. No saturation trend in resistance reduction is observed even at the highest pressure of 87 GPa, indicating that BiOCuSe undergoes pressure-induced metallization in extremely high-pressure regions. However, no signature

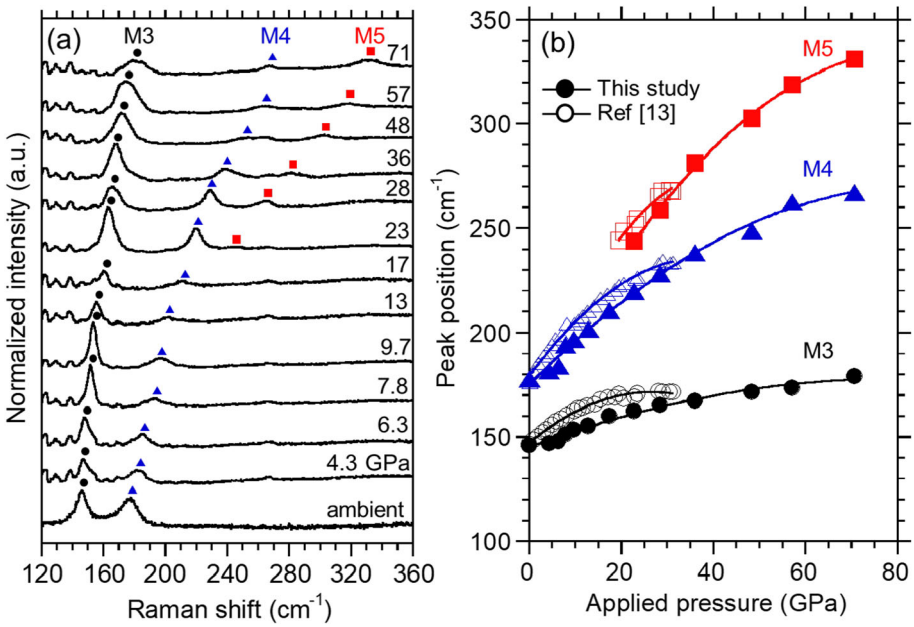

Fig. 4 **a** Raman spectra under various pressures. **b** Pressure dependence in the peak positions of Raman active modes of M3, M4, and M5

of superconductivity is detected at the maximum pressure applied in this study. Further experiments with higher pressures, potentially using smaller culet diameters in diamond anvils, are necessary to explore the possibility of pressure-induced superconductivity.

Figure 4a presents the Raman spectra of BiOCuSe under various pressures. At ambient pressure, two Raman-active modes, $A_{1g}{}^1$ and $A_{1g}{}^2$, labeled as M3 and M4, respectively, are observed within the measurement range [13]. These modes correspond to out-of-plane vibrations of Bi and Se. At ambient pressure, the M3 and M4 modes are clearly identified at 145.6 and 176.6 cm^{-1}, respectively. According to previous reports on the high-pressure behavior of Raman-active modes [13], the M3 and M4 peaks gradually shift to higher wavenumbers due to phonon hardening, and an additional M5 peak emerges above 18.3 GPa. Moreover, synchrotron XRD measurements under high pressure, as reported in the literature, indicate no structural phase transition at least up to 31.6 GPa. In our Raman analysis, the pressure-dependent spectral changes, including the emergence of the M5 mode, are fully consistent with previously reported behavior, as shown in Fig. 4b. Furthermore, in the previously unexplored pressure range above 40 GPa, no new peaks appear in our data up to 71 GPa, indicating that no structural phase transition occurs in BiOCuSe within this pressure range.

Although the signature of metallization in BiOCuSe is observed at extremely high pressure, the diamond anvil was broken above 87 GPa, and the pressure naturally decreased to ambient condition. Instead of further increasing the pressure, we investigated the emergence of superconductivity by recompressing a BiOCuSe sample that had previously been compressed to 87 GPa and then recovered to ambient pressure. Figure 5a presents the R–T curves under various pressures from 2.3 to 8.4 GPa for the recovered BiOCuSe. At the lowest pressure, the sample exhibits metallic behavior from 300 to 150 K, followed by an upturn in resistance at lower temperatures. As the pressure up to 8.4 GPa, the semiconducting character, indicated by the negative slope of the R–T curve, becomes more pronounced, similar to the behavior observed in the first compression shown in Fig. 3b. However, above 10 GPa, the negative slope in the R–T curve decreases significantly, indicating the suppression of semiconducting behavior, as shown in Fig. 5b. At 25 GPa, a steep drop in resistance appears at low temperatures. Beyond 25 GPa, the slope of the R–T curve continues to decrease, and the sample exhibits nearly metallic behavior at 51 GPa. Figure 6a shows the normalized R–T curves in the low-temperature region above 25 GPa. The onset of the resistance drop shifts to higher temperatures with increasing pressure, and the transition becomes sharper. The plots of temperature dependence in dR/dT are presented in Fig. S1 to indicate onset temperature of the resistance drop. As shown in Fig. 6b, the resistance drop is systematically suppressed under applied magnetic fields, providing evidence for pressure-induced superconductivity in the recompressed sample. Figure 6c presents the pressure dependence of the T_c in recovered BiOCuSe. In our measurements, superconductivity emerges at 4.3 K at 25 GPa and rapidly increases to a maximum T_c of 5.8 K at 51 GPa. One possible origin of the observed superconductivity is the presence of elemental Se [35–37] as an impurity or byproduct due to partial decomposition during the initial compression up to 87 GPa. However, if the observed superconductivity were due to elemental Se, the pressure dependence of T_c would be expected to follow that of pure Se. In contrast, our results show a distinct pressure-dependent T_c trend [36], as indicated in Fig. 6c. Therefore, at this stage, we conclude that the observed superconductivity in recovered BiOCuSe

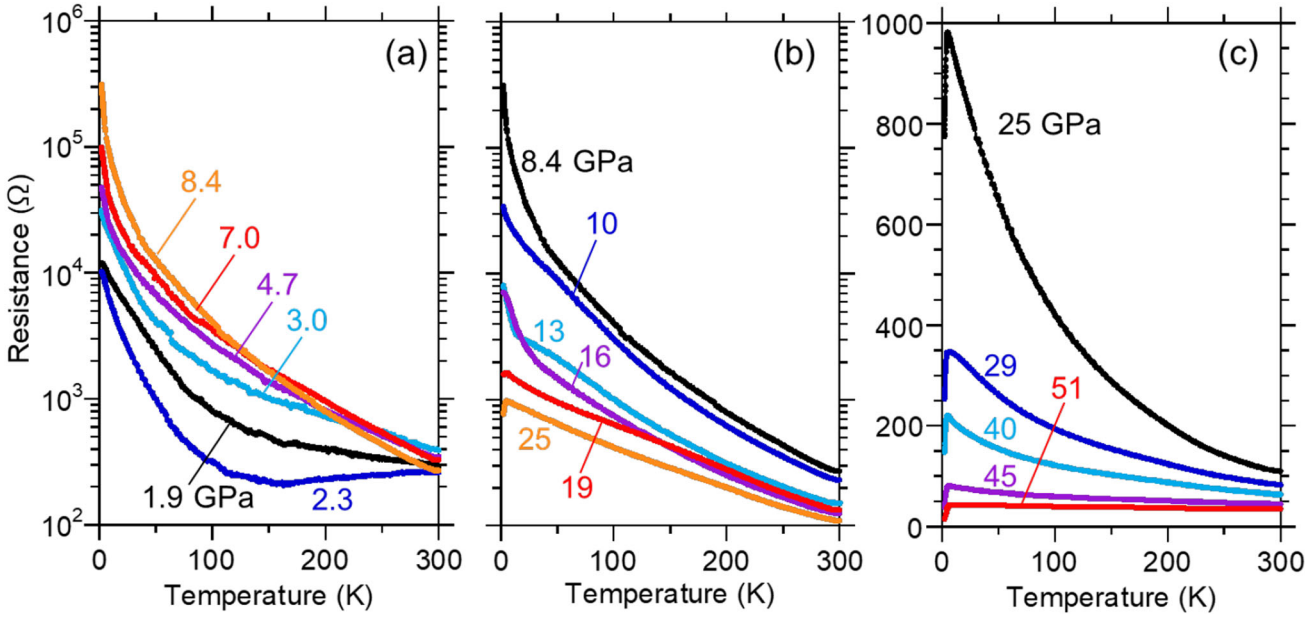

Fig. 5 **a** Temperature dependence of resistance under various pressures from 1.9 to 8.4 GPa in the recovered BiOCuSe which experiences the compression up to 87 GPa. **b** Pressure range of 8.4 to 25 GPa, and **c** 25 to 51 GPa

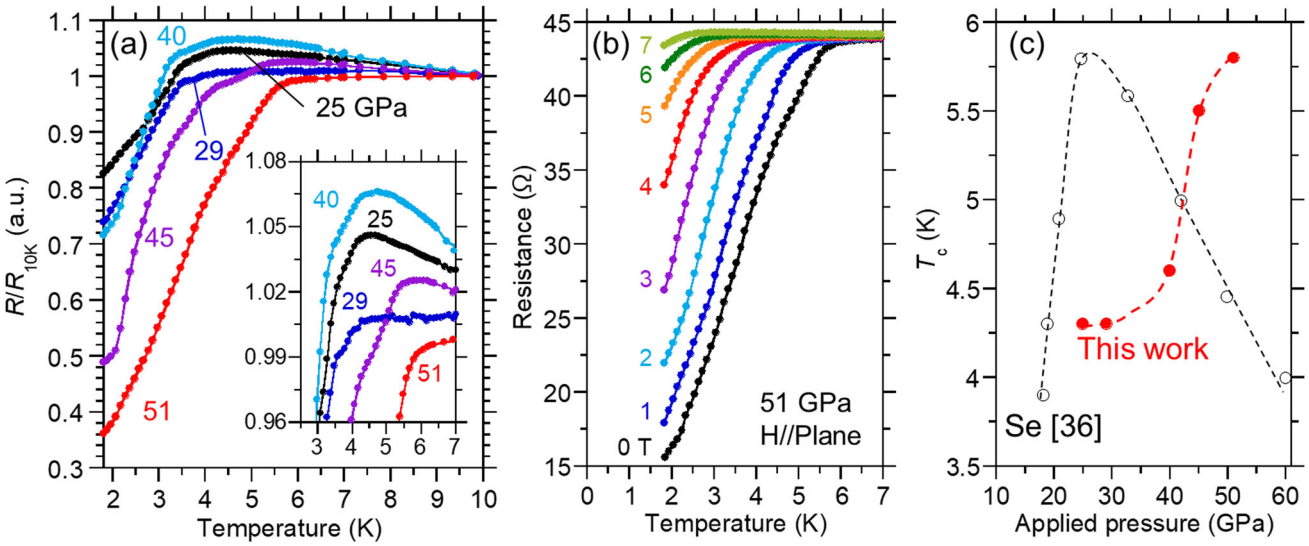

Fig. 6 **a** R–T properties in recovered BiOCuSe at low temperature region. **b** Magnetic field dependence of the drop of resistance at 51 GPa. **c** Pressure dependence in T_c with a comparison of that in elemental Se [36]

originates from BiOCuSe itself or an unknown derivative formed through decomposition, rather than from elemental Se.

Figure 7 presents the pressure dependence of the electrical resistance at 300 K (R_{300K}) in metallic BiOCuSe up to 87 GPa, compared to the data from previously studied semiconducting BiOCuSe [13]. For the initially semiconducting BiOCuSe, the resistivity decreases up to 10 GPa and then begins to increase as pressure is applied. In contrast, the initially metallic BiOCuSe shows an increasing trend of the resistance even below 10 GPa. The high-pressure behavior in the semiconducting BiOCuSe appears to shift to lower pressures in the metallic sample, likely due to differences in initial carrier concentration. The metallic nature of BiOCuSe is significantly suppressed by compression, with a metal-to-semiconductor transition occurring around 4 GPa. With further compression above 31 GPa, the semiconducting behavior is steeply suppressed, and the R_{300K} becomes lower than the ambient value above 60 GPa, indicating a semiconductor-to-metal transition. After releasing pressure from 87 GPa to ambient pressure, the initially metallic BiOCuSe is recompressed. The recovered sample exhibits a decreasing trend in resistance as a function of pressure, even near ambient pressure. The origin of the hysteresis effect

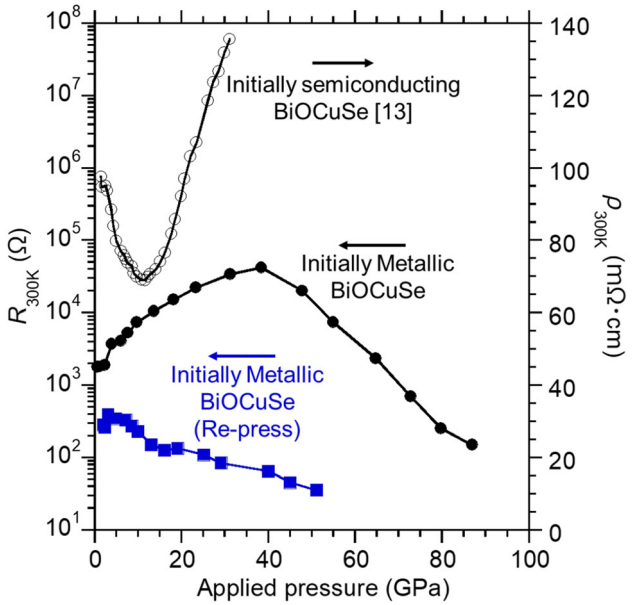

Fig. 7 Electrical resistance at 300 K (R_{300K}) as a function of pressure in initially metallic BiOCuSe and re-pressed one from this work and the resistivity at 300 K (ρ_{300K}) in initially semiconducting one from literature [13]

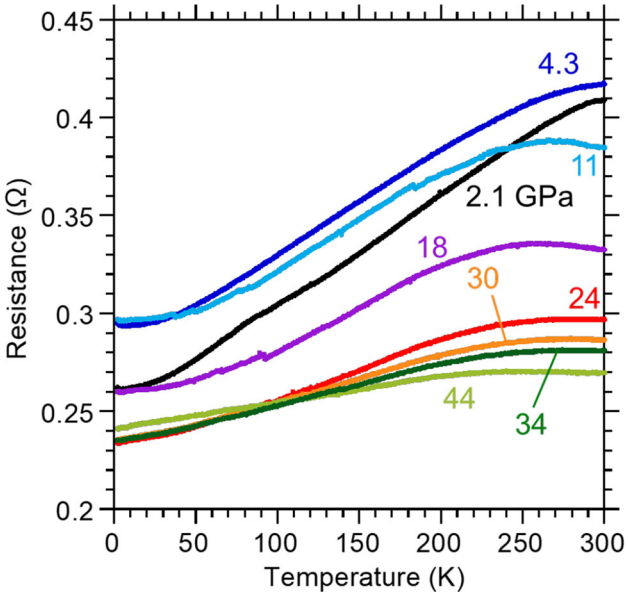

Fig. 8 Temperature dependence of resistance on $YBi_2O_4Cu_2Se_2$ under various pressures from 2.1 to 44 GPa

with respect to pressure application remains an open question. Although structural analyses using Raman spectroscopy and X-ray diffraction (XRD) are important, such measurements are challenging to perform on metallic single-crystalline samples. As a direction for future research, in-situ XRD measurements on polycrystalline samples under high pressure are expected to provide more accurate insights into the crystal structure. Furthermore, once the crystal structure of the superconducting phase is clarified, discussions on the superconducting pairing mechanism based on density functional theory (DFT) calculations becomes feasible.

4.2 $YBi_2O_4Cu_2Se_2$ and Cu_2Se

Figure 8 shows the temperature dependence of resistance in $YBi_2O_4Cu_2Se_2$ under various pressures ranging from 2.1 to 44 GPa. As observed in the R–T curve at ambient pressure, $YBi_2O_4Cu_2Se_2$ exhibits metallic behavior at the lowest pressure of 2.1 GPa. Although there are slight changes in the absolute value of the resistance and the slope of the R–T curve with applied pressure, no drastic change in electrical properties, such as a metal-to-semiconductor transition or the emergence of superconductivity, is observed up to 44 GPa. While $YBi_2O_4Cu_2Se_2$ shows no signature of superconductivity at this stage of research, exploring higher pressure regions remains valuable, particularly in light of the recently reported high T_c phase in highly compressed transition metal diborides above 100 GPa [3, 38, 39].

Figure 9a, b shows the temperature dependence of resistance in Cu_2Se under various pressures ranging from 5.5 to 80 GPa. At the lowest pressure of 5.5 GPa, Cu_2Se exhibits metallic behavior with a large hump around 120 K, attributed to the formation of CDW state, which is consistent with its transport properties at ambient pressure. As pressure is applied, the absolute value of resistance increases, and the slope of the R–T curve gradually becomes negative, indicating a pressure-induced semiconductor transition. In this region, the transition temperature of the CDW (T_{CDW}) increases with pressure. Under further compression, the resistance begins to decrease, and the semiconducting behavior is rapidly suppressed. The T_{CDW} also decreases with increasing pressure. Around 50 GPa, the R–T curve shows partial metallic behavior, and the CDW transition nearly disappears. This pressure-induced metal-to-semiconductor transition, followed by the recovery of metallic features beyond the semiconducting phase, is similar to the behavior observed in BiOCuSe. Instead of full metallicity and suppression of the CDW transition, a small drop in resistance is observed at low temperatures, and this transition is gradually suppressed under applied magnetic fields, as shown in Fig. 9c–f, indicating the emergence of superconductivity. Figure 10 presents the pressure phase diagram of Cu_2Se, showing the pressure dependence of R_{300K}, T_{CDW}, and T_c. Under the non-hydrostatic pressure conditions, the multi-step transition of superconductivity, due to a pressure distribution in the sample, is often observed. The T_c is determined using an onset temperature of the resistance drop. The T_{CDW} increases as the semiconducting feature is enhanced with increasing pressure up to 20 GPa. The metallic behavior progresses with a reduction in T_{CDW} above 20

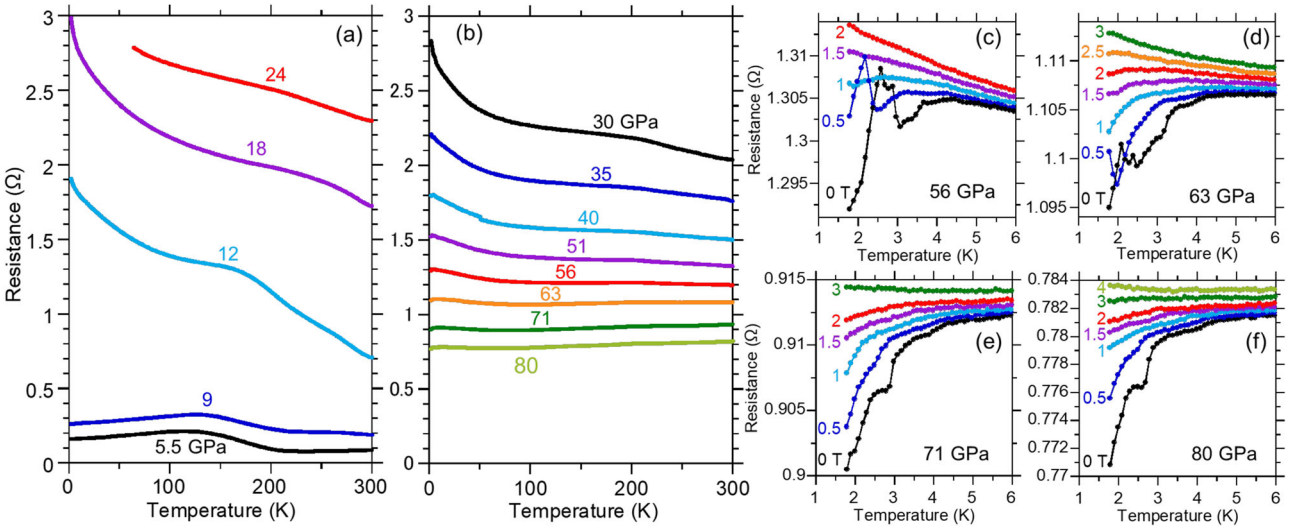

Fig. 9 Temperature dependence of resistance on Cu_2Se under various pressures from **a** 5.5 to 24 GPa, **b** 30 to 80 GPa. The enlarged plots around low-temperature regions under various magnetic fields are shown in **c** to **f**

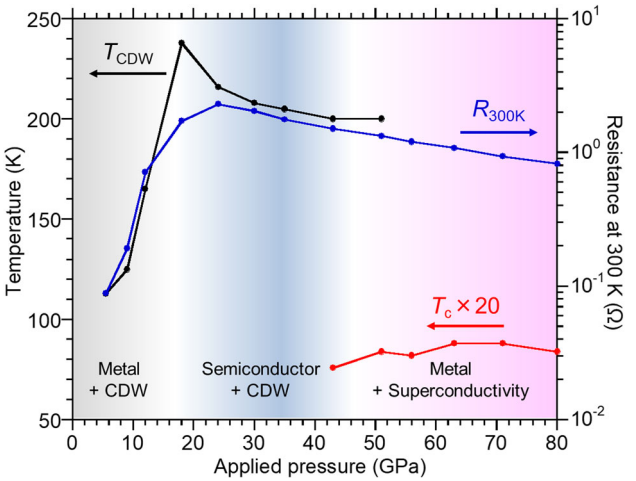

Fig. 10 Pressure dependence of the resistance at 300 K, the transition temperature in CDW, and the superconducting transition temperature in Cu_2Se

GPa. Under further compression, Cu_2Se exhibits metallic behavior without CDW features and shows superconductivity. The pressure-induced tuning of T_{CDW} and the subsequent emergence of superconductivity after the suppression of CDW has been observed in various materials, including transition metal chalcogenides [40], topological kagome metals [41, 42], and recently discovered high-T_c nickelates [4, 43]. The origin of the observed superconductivity, however, needs further investigation, as the transition is highly filamentary. In a current stage of research, the filamentary transition possibly originates from the non-hydrostatic pressure. While the observed T_c differs from reported values for elemental Se and other Cu–Se binary compounds, such as $CuSe_2$ [44], partial decomposition under extreme pressure may contribute to this effect.

5 Conclusion

The exploration of novel superconducting families is a crucial challenge in the search for next-generation high-T_c materials. One promising strategy is the examination of conducting layer replacements, which can be accelerated by combining high-pressure experiments, as demonstrated by the recent discovery of high-T_c nickelates. This study presents a series of electrical transport measurements under high pressure on CuSe-based compounds of BiOCuSe, $YBi_2O_4Cu_2Se_2$, and Cu_2Se using a custom-designed DAC with the BDD electrodes. The high-pressure effects on the electrical properties of these compounds are summarized as follows:

In BiOCuSe, metallic behavior rapidly disappears under pressure up to 3.9 GPa, and a semiconducting feature appears. The pressure-induced semiconducting nature is suppressed above 31 GPa, with metallic tendencies reappearing at higher pressures. While bulk superconductivity is not observed up to 87 GPa, the recovered and re-compressed BiOCuSe exhibits superconducting signals above 20 GPa. $YBi_2O_4Cu_2Se_2$, which remains metallic, shows a positive R–T curve up to 44 GPa without any anomalies in its electrical properties. Cu_2Se, initially exhibiting metallic behavior with a CDW transition at ambient pressure, changes to a semiconducting feature with an increase in T_{CDW} up to 24 GPa. At higher pressures, the CDW disappears, and metallic properties are recovered, with a filamentary superconducting transition emerging above 40 GPa.

Since the observed superconducting signals in BiOCuSe and Cu_2Se are filamentary, further microscopic analysis, such as in-situ XRD and other local observation techniques, is required to investigate the origin of superconductivity. Our findings open new directions for future research in the field of CuSe-based superconductors. Moreover, as our high-pressure experiments were limited to below 100 GPa, further investigations beyond

100 GPa, using advanced high-pressure techniques, are expected to provide insights into the potential emergence of high-T_c superconductivity. In addition, the carrier tuning in these compounds using a fabrication of the electric double layer transistor (EDLT) in the sample space of DAC [45] is promising strategy to induce superconductivity at ambient condition or lower pressure region.

Acknowledgements This work was partly supported by JSPS KAKENHI Grant Number 23H01835, 23K13549, and 23KK0088. The fabrication process of diamond electrodes was partially supported by the NIMS Nanofabrication Platform in the Nanotechnology Platform Project sponsored by the Ministry of Education, Culture, Sports, Science and Technology (MEXT), Japan. The calculations in this study were performed on the Numerical Materials Simulator at NIMS. The nano-polycrystalline diamond was synthesized and provided via the Visiting Researcher's Program of the GRC with proposal No. 2023YB01. This work was supported by the World Premier International Research Center Initiative (WPI), MEXT, Japan.

Author contributions

Ryo Matsumoto: conceptualization, methodology, investigation, and writing—original draft. Sayaka Yamamoto: investigation, visualization, and reviewing manuscript. Shintaro Adachi: investigation and reviewing manuscript. Hiromi Tanaka: investigation and reviewing manuscript. Toru Shinmei: investigation and reviewing manuscript. Tetsuo Irifune: investigation and reviewing manuscript. Yoshihiko Takano: supervision, funding acquisition, and reviewing manuscript.

Data availability statement The manuscript has no associated data. [Authors' comment: The data that support the findings of this study are available from the corresponding author, upon reasonable request.]

Code availability This study did not use any custom code or software that is not publicly available.

References

1. A.P. Drozdov, M.I. Eremets, I.A. Troyan, V. Ksenofontov, S.I. Shylin, Conventional superconductivity at 203 kelvin at high pressures in the sulfur hydride system. Nature **525**, 73 (2015)
2. M. Einaga, M. Sakata, T. Ishikawa, K. Shimizu, M.I. Eremets, A.P. Drozdov, I.A. Troyan, N. Hirao, Y. Ohishi, Crystal structure of the superconducting phase of sulfur hydride. Nat. Phys. **12**, 835 (2016)
3. C. Pei et al., Pressure-induced superconductivity at 32 K in MoB2. National Sci. Rev. **10**, nwad034 (2023)
4. H. Sun et al., Signatures of superconductivity near 80 K in a nickelate under high pressure. Nature **621**, 493 (2023)
5. H. Sakakibara et al., Theoretical analysis on the possibility of superconductivity in the trilayer Ruddlesden–Popper nickelate $La_4Ni_3O_{10}$ under pressure and its experimental examination: comparison with $La_3Ni_2O_7$. Phys. Rev. B **109**, 144511 (2024)
6. A.P. Drozdov et al., Superconductivity at 250 K in lanthanum hydride under high pressures. Nature **569**, 528 (2019)
7. M. Somayazulu, M. Ahart, A.K. Mishra, Z.M. Geballe, M. Baldini, Y. Meng, V.V. Struzhkin, R.J. Hemley, Evidence for superconductivity above 260 K in lanthanum superhydride at megabar pressures. Phys. Rev. Lett. **122**, 027001 (2019)
8. P. Kong et al., Superconductivity up to 243 K in the yttrium-hydrogen system under high pressure. Nat. Commun. **12**, 5075 (2021)
9. N.P. Salke et al., Synthesis of clathrate cerium superhydride CeH_9 at 80–100 GPa with atomic hydrogen sublattice. Nat. Commun. **10**, 4453 (2019)
10. T. Chou, G.C. Tewari, T. Chan, Y. Hsu, J. Chen, H. Yamauchi, M. Karppinen, Semiconducting BiO-CuSe thermoelectrics and its metallic derivative $Bi_2YO_4Cu_2Se_2$. Eur. J. Inorg. Chem. **2015**, 2574 (2015)
11. C. Barreteau, D. Bérardan, L. Zhao, N. Dragoe, Influence of Te substitution on the structural and electronic properties of thermoelectric BiCuSeO. J. Mater. Chem. A **1**, 2921 (2013)
12. Y. Liu et al., Remarkable enhancement in thermoelectric performance of BiCuSeO by Cu deficiencies. J. Am. Chem. Soc. **133**, 20112 (2011)
13. Q. Zhang et al., Pressure impact on the crystal structure, optical, and transport properties in layered oxychalcogenides BiCu *Ch*O(*Ch* = S, Se). J. Phys. Chem. C **122**, 15929 (2018)
14. Iron-based layered superconductor $La[O_{1-x}F_x]FeAs$ ($x = 0.05-0.12$) with $T_c = 26$ K. https://doi.org/10.1021/ja800073m
15. D.D. Fan, H.J. Liu, L. Cheng, J. Zhang, P.H. Jiang, J. Wei, J.H. Liang, J. Shi, Understanding the electronic and phonon transport properties of a thermoelectric material BiCuSeO: a first-principles study. Phys. Chem. Chem. Phys. **19**, 12913 (2017)
16. Y. Xiao, Y. Pei, C. Chang, X. Zhang, X. Tan, X. Ye, S. Gong, Y. Lin, J. He, L.-D. Zhao, Electrical and thermal transport properties of layered $Bi_2YO_4Cu_2Se_2$. J. Solid State Chem. **239**, 178 (2016)
17. S.G. Tan, D.F. Shao, W.J. Lu, B. Yuan, Y. Liu, J. Yang, W.H. Song, H. Lei, Y.P. Sun, CuSe-based layered

compound $Bi_2YO_4Cu_2Se_2$ as a quasi-two-dimensional metal. Phys. Rev. B **90**, 085144 (2014)
18. J. Cheng et al., Superconductivity in a layered cobalt oxychalcogenide Na_2CoSe_2O with a triangular lattice. J. Am. Chem. Soc. **146**, 5908 (2024)
19. D. Byeon et al., Discovery of colossal Seebeck effect in metallic Cu_2Se. Nat. Commun. **10**, 72 (2019)
20. M. Yao, W. Liu, X. Chen, Z. Ren, S. Wilson, Z. Ren, C.P. Opeil, Anomalous CDW ground state in Cu_2Se: a wave-like fluctuation of the DC I–V curve near 50 K. J. Materiomics **3**, 150 (2017)
21. P. Lu, H. Liu, X. Yuan, F. Xu, X. Shi, K. Zhao, W. Qiu, W. Zhang, L. Chen, Multiformity and fluctuation of Cu ordering in Cu_2 Se thermoelectric materials. J. Mater. Chem. A **3**, 6901 (2015)
22. Y. Zhang, X. Shao, Y. Zheng, L. Yan, P. Zhu, Y. Li, H. Xu, Pressure-induced structural transitions and electronic topological transition of Cu_2Se. J. Alloy. Compd. **732**, 280 (2018)
23. W. Liu, L. Yang, Z. Chen, J. Zou, Promising and eco-friendly Cu_2X-based thermoelectric materials: progress and applications. Adv. Mater. **32**, 1905703 (2020)
24. Y. Seto, D. Hamane, T. Nagai, K. Fujino, Fate of carbonates within oceanic plates subducted to the lower mantle, and a possible mechanism of diamond formation. Phys. Chem. Miner. **35**, 223 (2008)
25. K. Momma, F. Izumi, VESTA 3 for three-dimensional visualization of crystal, volumetric and morphology data. J. Appl. Crystallogr. **44**, 1272 (2011)
26. R. Matsumoto, Y. Nishizawa, N. Kataoka, H. Tanaka, H. Yoshikawa, S. Tanuma, K. Yoshihara, Reproducibility of XPS analysis for film thickness of SiO_2/Si by active Shirley method. J. Electron Spectrosc. Relat. Phenom. **207**, 55 (2016)
27. R. Matsumoto, Y. Sasama, M. Fujioka, T. Irifune, M. Tanaka, T. Yamaguchi, H. Takeya, Y. Takano, Note: Novel diamond anvil cell for electrical measurements using boron-doped metallic diamond electrodes. Rev. Sci. Instrum. **87**, 076103 (2016)
28. R. Matsumoto, T. Irifune, M. Tanaka, H. Takeya, Y. Takano, Diamond anvil cell using metallic diamond electrodes. Jpn. J. Appl. Phys. **56**, 05FC01 (2017)
29. R. Matsumoto, A. Yamashita, H. Hara, T. Irifune, S. Adachi, H. Takeya, Y. Takano, Diamond anvil cells using boron-doped diamond electrodes covered with undoped diamond insulating layer. Appl. Phys. Express **11**, 053101 (2018)
30. T. Irifune, A. Kurio, S. Sakamoto, T. Inoue, H. Sumiya, Ultrahard polycrystalline diamond from graphite. Nature **421**, 599 (2003)
31. H.K. Mao, P.M. Bell, J.W. Shaner, D.J. Steinberg, Specific volume measurements of Cu, Mo, Pd, and Ag and calibration of the ruby R1 fluorescence pressure gauge from 0.06 to 1 Mbar. J. Appl. Phys. **49**, 3276 (1978)
32. Y. Akahama, H. Kawamura, High-pressure Raman spectroscopy of diamond anvils to 250GPa: method for pressure determination in the multimegabar pressure range. J. Appl. Phys. **96**, 3748 (2004)
33. H. Singh, D. Prendergast, M. Nath, Modulation of electrocatalytic activity by tuning anion electronegativity: case study with copper chalcogenides. J. Phys. Energy **5**, 045016 (2023)
34. S.-T. Dong, Y.-Y. Lv, B.-B. Zhang, F. Zhang, S. Yao, Y.B. Chen, J. Zhou, S.-T. Zhang, Z.-B. Gu, Y.-F. Chen, Strong correlation of the growth mode and electrical properties of BiCuSeO single crystals with growth temperature. CrystEngComm **17**, 6136 (2015)
35. Y. Akahama, M. Kobayashi, H. Kawamura, Pressure-induced superconductivity and phase transition in selenium and tellurium. Solid State Commun. **84**, 803 (1992)

36. E. Gregoryanz, V. Struzhkin, R. Hemley, M. Eremets, H. Mao, Y. Timofeev, Superconductivity in the chalcogens up to multimegabar pressures. Phys. Rev. B **65**, 064504 (2002)
37. K. Shimizu, Superconductivity from insulating elements under high pressure. Physica C Supercond. Appl. **514**, 46 (2015)
38. J. Lim et al., Creating superconductivity in WB2 through pressure-induced metastable planar defects. Nat. Commun. **13**, 7901 (2022)
39. C. Pei et al., Pressure-induced superconductivity in itinerant antiferromagnet CrB2 (n.d.)
40. S. Sahoo, U. Dutta, L. Harnagea, A.K. Sood, S. Karmakar, Pressure-induced suppression of charge density wave and emergence of superconductivity in 1T−VSe_2. Phys. Rev. B **101**, 014514 (2020)
41. T. Neupert, M.M. Denner, J.-X. Yin, R. Thomale, M.Z. Hasan, Charge order and superconductivity in kagome materials. Nat. Phys. **18**, 137 (2022)
42. Z. Zhang et al., Pressure-induced reemergence of superconductivity in the topological kagome metal CsV_3Sb_5. Phys. Rev. B **103**, 224513 (2021)
43. G. Wang et al., Pressure-induced superconductivity in polycrystalline $La_3Ni_2O_{7-\delta}$. Phys. Rev. X **14**, 011040 (2024)
44. Y. Takano, N. Uchiyama, S. Ogawa, N. Môri, Y. Kimishima, S. Arisawa, A. Ishii, T. Hatano, K. Togano, Superconducting properties of $CuS_{2-x}Se_x$ under high pressure. Physica C **341–348**, 739 (2000)
45. S. Adachi et al., Demonstration of electric double layer gating under high pressure by the development of field-effect diamond anvil cell. Appl. Phys. Lett. **116**, 223506 (2020)